

# Journal of Materials Chemistry A

Accepted Manuscript



This is an *Accepted Manuscript*, which has been through the Royal Society of Chemistry peer review process and has been accepted for publication.

*Accepted Manuscripts* are published online shortly after acceptance, before technical editing, formatting and proof reading. Using this free service, authors can make their results available to the community, in citable form, before we publish the edited article. We will replace this *Accepted Manuscript* with the edited and formatted *Advance Article* as soon as it is available.

You can find more information about *Accepted Manuscripts* in the [Information for Authors](#).

Please note that technical editing may introduce minor changes to the text and/or graphics, which may alter content. The journal's standard [Terms & Conditions](#) and the [Ethical guidelines](#) still apply. In no event shall the Royal Society of Chemistry be held responsible for any errors or omissions in this *Accepted Manuscript* or any consequences arising from the use of any information it contains.



Journal Name

ARTICLE

## Well-controlled Layer-by-Layer Assembly of Carbon Dots/CdS Heterojunction for Efficient Visible-Light-Driven Photocatalysis

Na-Na Chai,<sup>a</sup> Hang-Xing Wang,<sup>a</sup> Chen-Xia Hu,<sup>a</sup> Qiang Wang\*<sup>b</sup> and Hao-Li Zhang\*<sup>a</sup>Received 00th January 20xx,  
Accepted 00th January 20xx

DOI: 10.1039/x0xx00000x

www.rsc.org/

**Abstract:** Fluorescent carbon dots have attracted great attention, but the application in photocatalysis has not been well explored. Herein we report a facile layer-by-layer method to fabricate uniform C dots/CdS heterojunction films via electrophoretic and sequential chemical bath deposition method. Because no ligands are used, the strategy facilitates the formation of intimate interfacial contact beneficial for charge separation and transfer, which can lead to a high photocurrent density of 2.6 mA·cm<sup>-2</sup>. In addition, the electron donor-acceptor heterojunction can expedite charge separation and effectively suppress electron-hole pair recombination, eventually contributing to enhanced photoelectrochemical and/or photocatalytic efficiency of the system. As a proof-of-concept, the hybrid films manifested themselves as efficient visible-light-driven photocatalyst when applied for reduction of nitro-benzene derivatives in aqueous phase under low power irradiation. Our findings thus establish a new frontier on the rational design and fabrication of well-controlled hybrid films with built-in heterojunctions for solar light conversion.

### Introduction

Fluorescent carbon-based nanodots have recently attracted mounting interest because of their facile preparation,<sup>1</sup> excellent photo<sup>2</sup> and chemical stability and versatile applications in opto-electronic field<sup>3,4</sup> and biological imaging.<sup>2, 3, 5-7</sup> Compared with two-dimensional (2D) zero bandgap graphene, 0-dimensional (0D) carbon dots (C dots) has intrinsic bandgap and is more promising for photochemical reactions due to their high optical activities associated with quantum confinement and edge effects.<sup>4, 8-11</sup> Lately, C dots have been employed for photocatalytic applications owing to their adjustable size, composition and visible light response.<sup>12-14</sup> For instance, C dots/semiconductors composites were explored for photocatalytic pollutants degradation<sup>4, 8</sup> and hydrogen evolution.<sup>15</sup> It was suggested that a strong interfacial contact between the C dots and inorganic semiconductors facilitated efficient charge transfer and thus beneficial for high photocatalytic activity.<sup>15</sup>

Cadmium sulfide (CdS) is a well-established semiconductor materials employed for a wide range of applications, including optoelectronics, photovoltaics, photodetectors, and

photocatalysis.<sup>16-24</sup> With a bandgap of 2.4 eV, the absorption of CdS matches well with the visible regime of solar irradiation. Although they have been studied for decades, most CdS materials still suffer from poor photostability and low conversion efficiency stemming from rapid electron-hole recombination, which severely limit their further applications. Recently, researchers are making efforts in combining CdS quantum dots with various 2D nano materials such as graphene, MoS<sub>2</sub> and TiO<sub>2</sub> sheets, in the purpose of achieving enhanced photoconversion efficiency and improved stability.<sup>19, 21, 23-31</sup>

These facts prompted us to assemble CdS with 0D C dots in order to obtain synergistic effects and hence to achieve even better opto-electronic response. Our rationale is that integration of C dots into CdS films could form a novel heterojunction structure, which would facilitate spatial separation of the photoinduced generated electrons and holes and prohibit exciton recombination.<sup>15, 24</sup> Hence in this work, we employed a facile LBL method to manufacture uniform C dots/CdS nano-hybrid films by electrophoretic and sequential chemical bath deposition (S-CBD).<sup>2</sup> In comparison with conventional methods such as Langmuir-Blodgett deposition,<sup>32</sup> vacuum filtration,<sup>33</sup> drop casting,<sup>34</sup> dip coating,<sup>35</sup> Our method enable the formation of a well-controlled assembly of C dots/CdS multilayers with intimate interfacial contact, which is beneficial for charge separation and transfer. The well-controlled assembly of C dots/CdS multilayers herein demonstrated stable and superior photoelectrochemical and/or photocatalytic performance upon visible light

<sup>a</sup> State Key Laboratory of Applied Organic Chemistry (SKLAOC), College of Chemistry and Chemical Engineering, Lanzhou University, Lanzhou, 730000, China. E-mail: haoli.zhang@lzu.edu.cn

<sup>b</sup> State Key Laboratory of Applied Organic Chemistry (SKLAOC), College of Chemistry and Chemical Engineering, Lanzhou University, Lanzhou, 730000, China. E-mail: qiangwang@lzu.edu.cn

Electronic Supplementary Information (ESI) available: Table S1-S2, Fig. S1-S13, See DOI: 10.1039/x0xx00000x

irradiation, indicative of promising applications in the solar light conversion field.

## Experiment section

### Materials and Characterization

All of the reagents and materials were obtained commercially, and were of analytical grade. Ultrapure water was produced by Millipore, Billerica, MA, U.S.

UV-Vis absorption spectra were recorded using a T6 UV-Vis spectrometer (Purkinje General, China). Photoluminescent spectra were operated on a FLS920 steady/transient fluorescence spectrometer (Edinburgh Instruments, U.K.). Photoelectrochemical measurements were carried out on a CHI 660b (CHI USA) electrochemical station. The Fourier transform infrared (FTIR) spectra were obtained on a Vertex 70v FTIR spectrophotometer (BRUKER USA). X-ray powder diffraction (XRD) patterns were obtained on a Panalytical X'Pert PRO. X-Ray photoelectron spectroscopy (XPS) data were measured by an Axis Ultra DLD system having an Al K source. Scanning electron microscopy (SEM) studies were performed using Hitachi S-4800 operated at 5kV, 10 $\mu$ A. Transmission electron microscopy (TEM) studies were performed using a TECNAI G2 F30 (FEI) operated at 300 kV. The TEM samples were prepared by dropping solution onto ultra-thin carbon membrane and dried in air. Atomic force microscopy (AFM) measurements were conducted in air by tapping-mode on an Agilent 5500 SPM. The samples were prepared by drop-casting 1mL suspension on freshly cleaved mica surface and dried in air.

### Synthesis of C dots

The synthesis of C dots adopted a pyrolysis method similar to that reported by Liu et al.<sup>4</sup> L-cysteine (1 g, 8.25 mmol) were added into 25ml beaker, then the beaker was transferred into electric oven and heated at 280 $^{\circ}$ C for 5 min (Fig. S3 $\dagger$ ). Thereafter, the beaker was cooled to room temperature, and the final product was collected by adding ultrapure water into the beaker and centrifuged at 8000 rpm for 5 min. The supernatant can be collected by rotary evaporation.

### Synthesis of L-cysteine-capped-CdS nanoparticles

Water-solution CdS nanoparticles were synthesized according to the method reported previously.<sup>36</sup> 110 mg L-cysteine was added to 25 ml of 1 mol $\cdot$ l $^{-1}$  Tris buffer that was argon-saturated and thoroughly degassed, to the mixture 15 ml of 0.01 mol $\cdot$ l $^{-1}$  of CdCl<sub>2</sub> aqueous solution was added, resulting in an L-cysteine/Cd molar ratio of 3:1. Then, 95  $\mu$ l of 0.4 mol $\cdot$ l $^{-1}$  Na<sub>2</sub>S $\cdot$ 9H<sub>2</sub>O solution was slowly added into the solution to afford an S/Cd molar ratio of 0.25:1. The mixed solution was stirred for 1 h at room temperature, followed by 10 min of flushing with argon to remove the unreacted sulfide. To remove L-cysteine-Cd complexes, the L-cysteine-capped-CdS (L-capped-CdS) nanoparticles were precipitated by adding cool ethanol to the reaction mixture of room temperature. The nanoparticles were dissolved in pure water, and precipitated

again with cool ethanol. The resulting L-capped-CdS nanoparticles were dried overnight under vacuum at 40 $^{\circ}$ C for further experiments.

### Self-Assembly of the C dots/CdS Multilayered Films

Electrophoretic deposition was performed using a custom-built reaction equipment with three electrodes: a ITO-coated glass electrode (deposition area: 1.0 cm $\times$ 0.75 cm, the actual photocatalyst quality: 0.33 mg), platinum electrode and the saturated calomel electrode. The ITO glasses was pre-cleaned by detergent, and then rinsed with plenty of water, followed by sonication with pure water, ethanol, acetone and isopropanol for 15 min, respectively. The C dots were then deposited onto the ITO substrate at a constant voltage of 10 V in 1 mg $\cdot$ ml $^{-1}$  C dots aqueous solution for a desired time. After electrophoretic deposition, the C dots-coated ITO glass was withdrawn from the solutions and washed with ultrapure water, then dried in air at room temperature.

To directly synthesize CdS QDs from aqueous solution without any ligand, sequential chemical bath deposition (S-CBD)<sup>7</sup> method was applied. The C dots-coated ITO glass was successively immersed in four different beakers for about 30 seconds in each beaker. One beaker contained 0.05 M CdCl<sub>2</sub> aqueous solution, and another contained 0.05 M Na<sub>2</sub>S aqueous solution, and the other two contained ultrapure water to remove excess precursor solution. Such a cycle was repeated 20 times, which receive a yellow film with a thickness of 180 nm. When the bath deposition cycle was further increased, the CdS nanosheets appeared aggregation on the ITO glass. Layered C dots/CdS photoelectrodes were prepared by repeating these two steps of electrophoretic deposition and S-CBD.

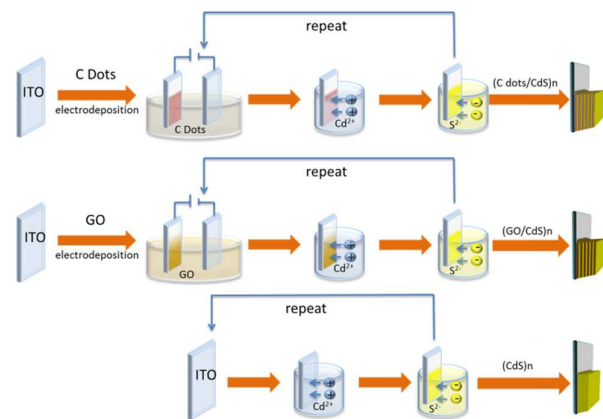
### Photocurrent response

Photoelectrochemical measurements were carried out in a custom-made three-electrode quartz cell in which platinum wire was used as a counter electrode, saturated calomel electrode as a reference electrode, and the ITO samples as the working electrodes. An aqueous Na<sub>2</sub>S solution (0.05 M) was chosen as the electrolyte and a 500 W xenon arc lamp (in a distance of 30 cm, with power density of 43 mW $\cdot$ cm $^{-2}$ ) was applied as the light source.

### Photocatalytic experiment

The photocatalytic experiment, a 3W LED lamp equipped with a UV cutoff filter ( $\lambda > 420$  nm) was used as a low energy-consuming visible light source. In a round bottom flask (25 ml), the ITO samples with active area of around 75 mm $\times$ 100 mm were immersed into 15 mL aqueous solution (10 mg $\cdot$ L $^{-1}$ ) of aromatic nitro compounds along with 20 mg of HCOONH<sub>4</sub>. Before irradiation, the solution was stirred in dark for 30 min to ensure an adsorption-desorption equilibrium between the photocatalyst and reactant. The reaction was monitored by UV-Vis spectra. The whole experimental process was conducted under N<sub>2</sub> atmosphere at ambient conditions.

## Results and discussion



Scheme 1. Schematic illustration for the layer-by-layer assembly of C dots/CdS, GO/CdS, and pure C dots multilayered films.

The layer-by-layer (LBL) assembly process for preparing the heterojunction films is illustrated in Scheme 1. Taking advantage of the excellent controllability of the strategy, C dots/CdS multilayers with various layer numbers and thickness can be conveniently constructed. In order to reveal the role of the C dots in photocatalysis, we have fabricated two other types of photoactive electrodes, including graphene oxide (GO)/CdS multilayer and CdS thin film. The classic photocatalytic electrode of CdS is used as a reference here. Meanwhile, GO has been widely studied for various photoelectrochemical applications.<sup>37</sup> A comparison between the GO/CdS and C dots/CdS heterojunctions fabricated under similar condition shall help to identify which carbon-based nanomaterial is more efficient for photocatalysis applications.

Electrostatic interaction is a key factor for manufacturing the heterojunction multilayers. The ITO substrate was hydrophilic in nature. Initially, the negatively charged C dots

was electrodeposited on the surface of ITO at 10V, and the positively charged  $\text{Cd}^{2+}$  ions subsequently adsorbed onto the C dots film. As a result, the negatively charged  $\text{S}^{2-}$  ions could quickly adsorb  $\text{Cd}^{2+}$  ions via electrostatic interactions to form CdS QDs thin film. By repeating the above steps, the well-controlled uniform C dots/CdS QDs hybrid multilayered film was constructed.

N-S-doped C dot is used in this work, as previous research has suggested N-S-doping could significantly enhance the photoemission properties of carbon dots.<sup>2</sup> Herein the C dot is prepared by direct carbonization of organic precursors (L-cysteine) in solid state based on a modified procedure from previous reports.<sup>38</sup> Transmission electron microscope (TEM) images of the as-synthesized C dots are shown in Fig. 1a, which are well-dispersed, and exhibit near-spherical morphology with uniform size distribution. According to the histogram (inset Fig. 1a), the average size of the C dots is measured to be about 3.6 nm. Meanwhile, the C dot displays lattice spacing of 0.21 nm in high resolution TEM images (Fig. 1b), consistent with the (100) lattice fringes of graphene. The AFM images further confirm the uniform of the C dots, and indicate that the average thickness of the C dots is below 2 nm (Fig. 1c). X-ray photoelectron spectroscopy (XPS) was employed to determine the composition of the C dots. As shown in Fig. 1d, three peaks at 533, 400, and 284 eV, correspond to O 1s, N 1s and C 1s, respectively. Additional peaks at 227 and 164 eV are found in the full survey of S, which were attributed to S 2s and S 2p peak, respectively. The observation verifies that the C dots are successfully doped with N and S elements. In addition, GO was synthesized from natural graphite using a modified Hummers method as we reported before,<sup>39,40</sup> which has also been characterized by TEM, AFM and XPS data (Fig. 1). The TEM image of GO (Fig. S2†) reveals that the graphene oxide sheets mostly exist as large thin sheets with the width of several microns. Slight corrugations are also observed due to the extremely large aspect ratio of the sheet. Typical AFM topography image (Fig. S2b†) indicates that the contrast of platelets is very uniform except for the isolated wrinkles and protrusions, with the corresponding line profile showing a monolayer thickness of  $\sim 1.0$  nm. XPS spectra of GO in Fig. S2c† only exhibit two peaks at 533 and 284 eV, corresponding to O 1s and C 1s, respectively. No S and N signals are observed for the GO sample.

Fig. 2a shows the FT-IR spectra of C dots in comparison with that of GO. Similar to GO, the distinct peaks at around 1730, 1645, 1397, 1075  $\text{cm}^{-1}$  are attributed to C=O, C=C stretching, C-H bending and C-O stretching modes, respectively, indicative of concomitant formation of these bonds during C dots growth. The digital image and UV-Vis absorption of the C dots and GO suspension in water are shown in Fig. 2b. The UV-Vis absorption of C dots bears certain resemblance to that of GO, extending to the visible range up to  $\sim 600$  nm, a property favourable for visible-light-driven photoactivity.

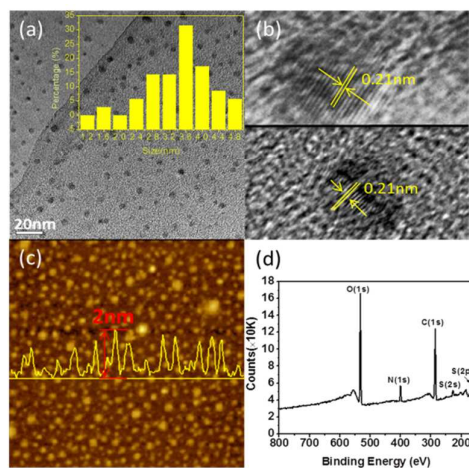


Fig. 1. TEM images of (a, b) C-dots, AFM images of (c) C-dots and (d) XPS spectra of C dots.

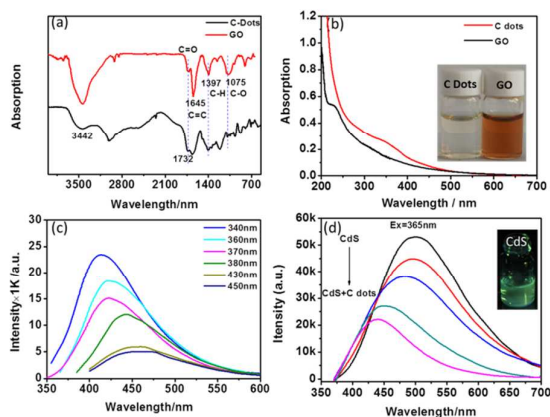


Fig. 2. (a) FTIR spectra of C dots and GO. (b) UV-vis absorption spectra of C dots and GO. (The inset images are C dots and GO solution under visible light irradiation) (c) Photoluminescent spectra of C dots and (d) Photoluminescence of CdS QDs and “CdS QDs + C dots” with increased C dots concentration under the excitation of 365nm. (Inset image is CdS QDs solution under UV light irradiation).

Fig. 2c exhibits the photoluminescence (PL) of the C dots. Clearly, when the excitation wavelength varies from 340 nm to 450 nm, the PL peaks also red shift and the intensity reaches a maximum when excited at 340 nm. The excitation-dependent emission phenomena is typical for C dots, as their surface state and the size effect induce complexity of the excited states.<sup>6</sup>

The construction of an effective heterojunction in the C dots/ CdS hybrid requires the occurrence of efficient charge transfer process. We thus examined the interplay of the individual components via steady-state fluorescence quenching in aqueous solution. The fluorescence spectra of the as-synthesized L-capped-CdS were shown in Fig. 2d. With continuous addition of C dots in the solution, the emission intensity of CdS was gradually quenched, implying possible electron transfer process from CdS QDs to C dots. This result was also confirmed by time-resolved fluorescence spectra (Fig. S1†). The decay profiles of CdS QDs and “CdS QDs + C dots” were fitted with multiexponential curves to derive three lifetime components for each. The averaged fluorescence lifetime was found to decrease from ~4 ns for CdS to ~3 ns of “CdS QDs + C dots”, further verifying the charge transfer process between them (Table S1†). Indeed, Mott-Schottky plots<sup>41,42</sup> estimated the conduction band (CB) edge of -0.37 V and -0.04 V (vs. NHE) for CdS QDs and C dots, respectively (Fig. S4†). The much lower-lying CB edge of C dots would render the electron transfer from CdS QDs to C dots and thus an efficient charge separated state.

The film morphology of the CdS QDs, GO/CdS QDs and C dots/CdS multilayer films are characterized by AFM (Fig. 3). The surface of CdS thin films was lumpy as a result of too much agglomerated CdS QDs on the surface (Fig. 3a). By contrast, the two hybrid films of C dots/CdS and GO/CdS showed

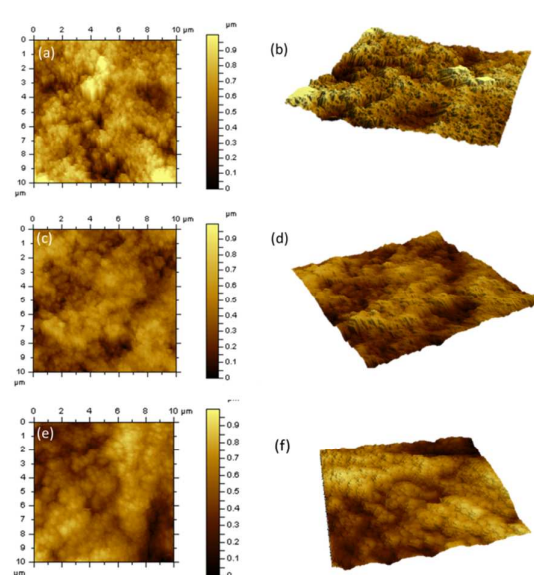


Fig. 3. AFM images and 3D images of (a, b) CdS QDs, (c, d) (GO/CdS)<sub>6</sub> composite films and (e, f) (C dots/CdS)<sub>6</sub> assembled on ITO substrate.

uniformly distributed surface with a tightly stacked morphology (Fig. 3c and e), reflecting that grafting of C dots or GO 2D planes on ITO substrate renders smoother CdS QDs deposition. The interconnected structure between carbon layer and CdS QDs may account for the close packing of these multilayered films. 3D AFM images of the three films illustrate even sharper contrast. As displayed in Fig. 3d and f, CdS QDs were closely and compactly assembled on the GO or C dots top layer, distinct from the morphology of pure CdS QDs film (Fig. 3b). Hence, AFM images strongly evidence the intimate

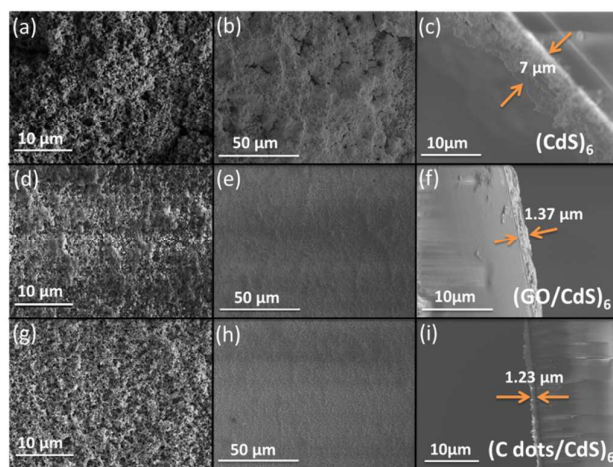


Fig. 4. Top view SEM images and cross-sectional SEM micrographs for hybrid films of (a, b, c) CdS QDs, (d, e, f) (GO/CdS)<sub>6</sub> and (g, h, i) (C dots/CdS)<sub>6</sub> assembled on ITO substrate.

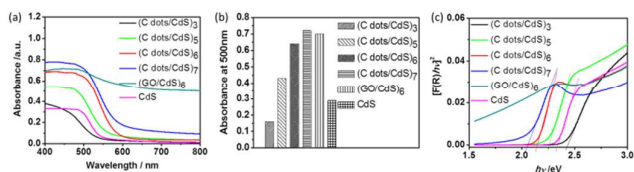


Fig. 5. UV-Vis diffuse reflectance spectra of (a) multilayers of pure CdS QDs, C dots/CdS hybrid films, and GO/CdS hybrid films (b) Absorption of multilayered films at wavelength of 500 nm. (c) Plot of  $[F(R)hv]^2$  versus  $hv$  for these hybrid multilayered thin films.

integration of CdS QDs and C dots or GO via the LBL-assembly build-up.

As shown in Fig. 4, the SEM images of pure CdS QDs thin film (Fig. 4a-c) exhibit obvious surface defects, which would not be beneficial for transporting of photogenerated electron-hole pairs. By contrast, over a large region of the substrate, the GO/CdS QDs and C dots/CdS QDs multilayered films with a distribution over 50 micrometres are uniformly spread on ITO substrate by electrodeposition and S-CBD method, and no obvious cracks are observed. Fig. 4c, f, i display cross section images of CdS QDs, GO/CdS QDs film and C dots/CdS QDs film, C dots/CdS QDs film being the thinnest whereas CdS QDs film the thickest. Further SEM measurements indicated these hybrid films became thicker with increasing deposition cycles (Fig. S5<sup>†</sup>). Among these three hybrid films, C dots/CdS QDs and GO/CdS QDs films exhibit rather smooth surfaces while those of pure CdS QDs film are clearly uneven as the QDs agglomerated on the ITO surface, which might potentially cause recombination of photogenerated electron-hole pairs of CdS and thus reduce photocatalytic activity.

The layered structure of C dots/ CdS was probed by SEM. The optimal time of 7 seconds for the C dots layer deposition corresponds to a thickness of only 3 nm, thus it is difficult to clearly identify a single C dots layer. However, the interface between every thicker layer of (C dots/ CdS) is distinguishable. For instance, the cross-sectional image of (C dots/CdS)<sub>4</sub> shows discernable multilayer structure, which is distinct from that of pure (CdS)<sub>4</sub> layer exhibiting no obvious interfaces within the structure (Fig. S6<sup>†</sup>).

UV-vis diffuse reflectance spectra were used to test the optical properties of the prepared hybrid films. It can be clearly seen from Fig. 5a that pure CdS QDs, multilayered films of GO/CdS and C dots/CdS all exhibit strong absorbance in visible light range, with GO/CdS even exhibiting a broader absorption extending to the infrared region. For C dots/CdS films with different deposition cycles (Fig. 5b), the absorbance intensity at 500 nm rises accordingly with the cycles increase. Tauc plots obtained via the transformation based on Kubelka–Munk function versus energy of light is shown in Fig. 5c.<sup>23</sup> The estimated bandgaps of the composite films C dots/CdS hybrid films with assembly cycles of 3, 5, 6, 7, and 6 layers of CdS, GO/CdS films are shown to be around 2.43 eV, 2.25 eV, 2.14 eV, 2.05 eV, 2.33 eV and 1.30 eV, respectively, in

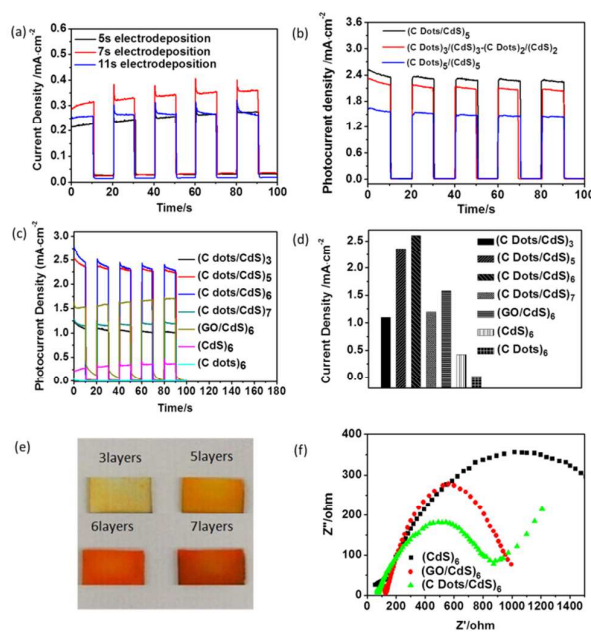


Fig. 6. (a) Photocurrent-time curves of (C dots/CdS)<sub>3</sub> with different C dots deposition time at the same three cycles. (b) Photocurrent-time curves of pure CdS QDs films, GO/CdS multilayered films and different deposition cycles of C dots/CdS multilayered film on glass ITO substrates in 0.05M Na<sub>2</sub>S aqueous solution under Xe light irradiation (43mW·cm<sup>-2</sup>). Applied potential: 0V vs SCE. (c) Transient photocurrent responses of these hybrid films in 0.05 M Na<sub>2</sub>S aqueous solution at zero bias versus Pt counter electrode under Xe light irradiation. (d) Photocurrent of multilayered films versus the number of deposition cycles. (e) Images of C dots/CdS multilayered films on glass ITO substrates. (f) Electrochemical impedance spectroscopy (EIS) Nyquist plots of CdS QDs film, GO/CdS and C dots/CdS multi-layered film with the same number of deposition cycles in 0.1 M Na<sub>2</sub>S aqueous solution at zero bias versus Pt counter electrode under 3W LED light irradiation; the amplitude of the sinusoidal wave was set at 5 mV, and the frequency varied from 100 kHz to 0.05 Hz.

Table S2<sup>†</sup>. This result indicates a bandgap narrowing with the increase of deposition cycles for the C dots/CdS hybrid film, which can be ascribed to increased interfacial interaction between CdS QDs and C dots that enhance electronic coupling. We also tested the UV-vis diffuse reflectance spectra of (C dots)<sub>6</sub> and (GO)<sub>6</sub>, the absorbance intensity of (C dots)<sub>6</sub> is higher than (GO)<sub>6</sub> at visible light range, this means that C dots can make full use of visible light (Fig. S7<sup>†</sup>). Fig. 6a shows transient photocurrent response for C dots/CdS hybrid films with three deposition cycles. The only difference is the deposition time of C dots. Clearly, the film with medium deposition time of 7s generates the largest photocurrent. Too long deposition time leads to thicker C dots layer, which increase photon absorption but may hinder the electron-hole pair separation from neighbored CdS layer and hence reduce the photocurrent of

hybrid films. While too short deposition time simply deteriorates light absorption of the layer and charge transfer with CdS. Thus it is of importance to balance photon absorption and separation of interfacial photogenerated electron-hole pairs. Specifically, the layer thickness can be roughly estimated by comparing with C dots layer deposited on ITO with a much longer deposition time of 120 second, which showed a thickness about 52 nm (Fig. S8†). Meanwhile, different stacking patterns between CdS QDs and C dots could also influence the photocurrent of these hybrid films (Fig. 6b). Consequently, a directly alternating deposition pattern between CdS and C dots, i.e., (C dots/CdS)<sub>n</sub>, is adopted in order to maximize the photocurrent output. Fig. 6c and d show transient photocurrent response for CdS QDs, C dots, and (C dots/CdS QDs)<sub>n</sub> (n = 3, 5, 6, 7) multilayered films under Xe lamp light irradiation (43 mW·cm<sup>-2</sup>) at zero bias condition. Obviously, the photocurrent of C dots/CdS hybrid film was enhanced significantly compared to that of pure CdS QDs, C dots films and GO/CdS with the same number of deposition cycles. Note that the largest photocurrent density of 2.6 mA·cm<sup>-2</sup> for (C dots/CdS)<sub>6</sub> is much higher than the values reported in relevant literatures.<sup>16, 20, 22, 23, 43</sup> In addition, the photocurrent density of (C dots/CdS)<sub>6</sub> can still reach a high value of 1.25 mA·cm<sup>-2</sup> even under sole visible light irradiation (3W LED irradiation, 15.4mW/cm<sup>2</sup>, λ>420nm, Fig. S9†). The observation can be attributed to the directly alternating deposition between CdS QDs and C dots, which leads to the formation of closely interfacial contact and renders the effective transfer of the photoexcited electrons in CdS QDs to the adjacent C dots film. Hence, C dots serve as efficient electron collector and transporter, and thus suppress recombination of photogenerated electron-hole pairs of CdS, in agreement with the above spectroscopic and Mott-Schottky plots evidence. In addition, the photocurrent of the C dots/CdS multilayered films increases gradually with the number of deposition cycles, reaches a maximum value of 2.6 mA·cm<sup>-2</sup> at 6 cycles, and then decreases with an even larger cycle number. This trend is possibly caused by the competition of photon absorption between CdS QDs and C dots,<sup>23, 44</sup> as is confirmed by measuring the photocurrent of composite films with different stacking methods illustrated in Fig. 6b. Fig. 6e is the digital images of the multilayered films with different deposition cycles. With increasing layer numbers, the color gradually deepens accordingly, indicative of mounting augment in visible light absorption.

We made supplemental photoelectrochemical experiments to test the photostability of the hybrid films up to 8 days (Fig. S10†). The photocurrent of pure CdS QDs film fell significantly to about 42% of its original values after 8 days, whereas the C dots/CdS hybrid film exhibited much more stable photocurrent output with 1.7% decrease. The result indicated that the C dots layer could effectively serve as a protective coating for the CdS QDs as well. We speculate that as C dots can act as electron acceptors, the electrons from conduct band of CdS upon photoexcitation can be efficiently immigrated to the surface of C dots. Through this electron transfer process, the

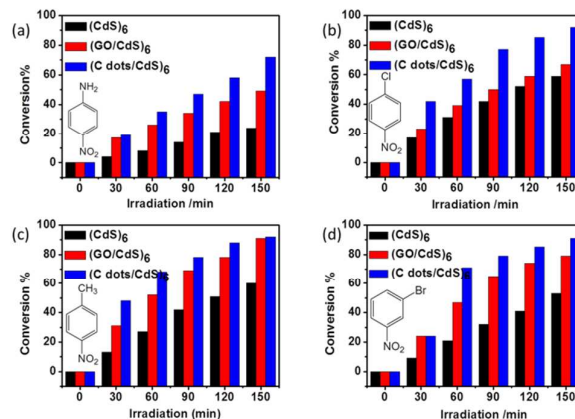


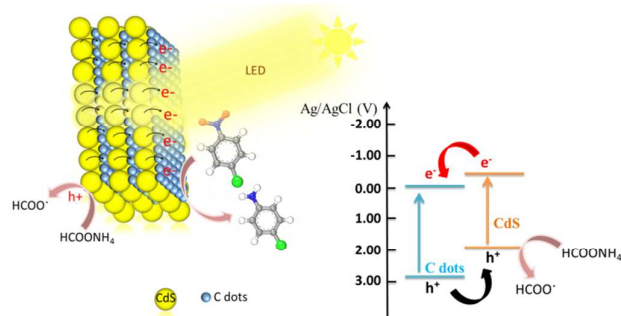
Fig. 7. Photocatalytic performances of the C dots/CdS QDs hybrid films were evaluated by photoreduction of nitroaromatic compounds to corresponding amino organics in aqueous phase under visible light irradiation.

photocorrosion of CdS may be curbed and the stability of (C dots/CdS)<sub>n</sub> layers is thus enhanced. The findings herein are in consistent with previous reports on the suppression of photocorrosion of photosensitizers via hybrid architectures.<sup>45, 46</sup>

To further understand the superior performance of C dots/CdS QDs multilayered film over GO/CdS QDs and pure CdS QDs in enhancing the transfer of photogenerated electron-hole charge carriers, electrochemical impedance spectroscopy (EIS)<sup>22, 23, 47</sup> as a method to monitor charge transfer process on the electrode and at the contact interface between electrode and electrolyte, was utilized to probe the frequency response of the electrode and electrolyte system. In Fig. 6f, the Nyquist plots show that C dots/CdS QDs multilayered films has smaller semicircle than that of GO/CdS QDs films with the same number of deposition cycles, which reveals more efficient interfacial electron transfer and faster electron transport process at the electrode-electrolyte interface for the former. The result explains although GO/CdS films exhibit broader absorption range, they generate a smaller photocurrent density than C dots/CdS QDs.

In summary, the enhanced photocurrent for the C dots/CdS hybrid film corroborates the role of C dots in promoting separation of photogenerated electron-hole pairs. Additionally, integration of C dots with CdS QDs based on layer-by-layer alternating deposition are beneficial for charge separation and transfer due to the formation of intimate interfacial contact, which also contribute to the photocurrent improvement. Moreover, more efficient charge transfer of the C dots/CdS films, as disclosed by EIS, implying they are of great potential for photocatalytic applications.

As a proof-of-concept, the C dots/CdS hybrid film was applied for photocatalytic reduction of nitro-benzene derivatives in aqueous phase under low power visible light irradiation. Using LED lamps as light sources offer several advantages such as high photon efficiency, low electrical power, high power stability, emission in broader spectral



Scheme 2. Proposed schematic mechanism for C dots/CdS involved photocatalytic process.

wavelengths, and no need for cooling during long time operation.<sup>48</sup> Photocatalytic reduction of p-nitroaniline on the C dots/CdS QDs film under a 3W LED light was presented as a typical example (Fig. S11<sup>†</sup>), which was monitored by the UV-vis light absorption spectra. Under the irradiation for 3 hours, the 380 nm absorption peak corresponding to p-nitroaniline vanished and new peaks at 300 and 240 nm appeared, indicating the formation of p-phenylenediamine. The products of this reduction reaction have also been confirmed by high performance liquid chromatography (HPLC). With prolonged reaction time to 6 hours, the reduction completed with a conversion rate as high as 99% (Fig. S11b<sup>†</sup>). Note the C dots/CdS QDs hybrid film demonstrated the best performance in comparison with GO/CdS and CdS QDs film with the same number of deposition cycles, in the order of C dots/CdS > GO/CdS > CdS QDs. For example, with the same reaction time of 2.5 hour, the conversion of p-nitroaniline using photocatalyst C dots/CdS is 70%, while that of GO/CdS is 49% and for CdS QDs the number is only 24%. The result from blank experiment under the same condition without photocatalyst is supplied in Fig. S12<sup>†</sup>. To test the photocatalytic activity of the films on various compounds, we studied three other different reactions (Fig. 7b, c, d) and all obtained similar trends, i.e., C dots/CdS films exhibited the best photocatalytic performance. All of these observation point to the crucial roles of C dots in the hybrid films for photocatalysis. To study the photostability of C dots/CdS QDs, three continuous recycling measurements were performed, where C dots/CdS QDs composite film exhibited high photoactivity and good photostability (Fig. S13<sup>†</sup>). In addition, it is noteworthy that the use of C dots/CdS QDs hybrid film as photocatalyst could avoid the tedious procedure of powder catalyst separation after photoreaction.

Based on the above results, a schematic mechanism for C dots/CdS involved photocatalytic application is provided in Scheme 2. Upon visible light irradiation, both C dots and CdS are excited and separated electrons and holes are thus generated within each entity. The lower-lying CB edge of C dots enable the electron transfer from CdS QDs to C dots, and concomitant movement of holes in the VB of C dots to that of CdS QDs. Consequently, efficient charge separated state is formed and the electrons thereafter lead to reduction

reactions. Meanwhile, sacrificial reagent replenishes electrons to make the photocatalytic cycle sustainable.

## Conclusions

To sum up, in this work a facile LBL method is adopted to manufacture uniform C dots/CdS nano-hybrid films, which demonstrate stable and superior photoelectrochemical and/or photocatalytic performance upon visible light irradiation. It is found the photocurrent density of the C dots/CdS hybrid film could reach  $2.6 \text{ mA}\cdot\text{cm}^{-2}$ , which is higher than ever reported in relevant literatures. Meanwhile, the films also showed efficient photocatalytic reduction of nitro-aromatic compounds to corresponding amino organics in aqueous phase under low power visible light irradiation. The significantly enhanced photoelectrochemical and/or photocatalytic efficiency of C dots/CdS were attributed to the following reasons: First, the combination of C dots with CdS form intimate interfacial contact and facilitate charge separation and transfer; Secondly, C dots herein act as efficient electron sinks, accepting photoinduced electrons from CdS and thus suppress electron-hole pair recombination. Last, the presence of C dots augments visible light absorption of the composites, leading to more photogenerated carriers and ultimate photocatalytic efficiency improvement. Our findings herein thus establish a new frontier on the rational design and fabrication of well-controlled hybrid films with built-in heterojunctions for solar light conversion. The conclusions section should come at the end of article, before the acknowledgements.

## Acknowledgements

This work is supported by National Basic Research Program of China (973 Program) No.2012CB933102, National Natural Science Foundation of China (NSFC. 21233001, 21190034, 21073079), Specialized Research Fund for the Doctoral Program of Higher Education (SRFDP. 20110211130001), the Fundamental Research Funds for the Central Universities and 111 Project.

## Notes and references

- 1 S. N. Baker and G. A. Baker, *Angew. Chem. Int. Ed.*, 2010, **49**, 6726.
- 2 Y. Q. Dong, H. C. Pang, H. B. Yang, C. X. Guo, J. W. Shao, Y. W. Chi, C. M. Li and T. Yu, *Angew. Chem. Int. Ed.*, 2013, **52**, 7800.
- 3 E. Lee, J. Ryu and J. Jang, *Chem. Commun.*, 2013, **49**, 9995.
- 4 J. H. Shen, Y. H. Zhu, X. L. Yang and C. Z. Li, *Chem. Commun. (Camb)*, 2012, **48**, 3686.
- 5 Y. Dong, C. Chen, X. Zheng, L. Gao, Z. Cui, H. Yang, C. Guo, Y. Chi and C. M. Li, *J. Mater. Chem.*, 2012, **22**, 8764.
- 6 S. J. Zhu, Q. N. Meng, L. Wang, J. H. Zhang, Y. B. Song, H. Jin, K. Zhang, H. C. Sun, H. Y. Wang and B. Yang, *Angew. Chem. Int. Ed.*, 2013, **52**, 3953.

- 7 C. X. Guo, H. B. Yang, Z. M. Sheng, Z. S. Lu, Q. L. Song and C. M. Li, *Angew. Chem. Int. Ed.*, 2010, **49**, 3014.
- 8 D. Qu, M. Zheng, P. Du, Y. Zhou, L. G. Zhang, D. Li, H. Q. Tan, Z. Zhao, Z. G. Xie and Z. C. Sun, *Nanoscale*, 2013, **5**, 12272.
- 9 D. Jiang, Y. Zhang, H. Chu, J. Liu, J. Wan and M. Chen, *RSC Adv.*, 2014, **4**, 16163.
- 10 K. Lingam, R. Podila, H. Qian, S. Serkiz and A. M. Rao, *Adv. Funct. Mater.*, 2013, **23**, 5062.
- 11 Q. Liu, B. Guo, Z. Rao, B. Zhang and J. R. Gong, *Nano Lett.*, 2013, **13**, 2436.
- 12 X. Yu, J. Liu, Y. Yu, S. Zuo and B. Li, *Carbon*, 2014, **68**, 718.
- 13 L. Feng, X. Y. Tang, Y. X. Zhong, Y. W. Liu, X. H. Song, S. L. Deng, S. Y. Xie, J. W. Yan and L. S. Zheng, *Nanoscale*, 2014, **6**, 12635.
- 14 D. K. Chan, P. L. Cheung and J. C. Yu, *Beilstein J. Nanotechnol.*, 2014, **5**, 689.
- 15 H. Yu, Y. Zhao, C. Zhou, L. Shang, Y. Peng, Y. Cao, L. Z. Wu, C. H. Tung and T. Zhang, *J. Mater. Chem. A*, 2014, **2**, 3344.
- 16 M. Fu, Q. Jiao and Y. Zhao, *RSC Adv.*, 2014, **4**, 23242.
- 17 P. Zeng, Q. Zhang, T. Peng and X. Zhang, *Phys. Chem. Chem. Phys.*, 2011, **13**, 21496.
- 18 L. Wu, Y. Zhang, X. Li and C. Cen, *Phys. Chem. Chem. Phys.*, 2014, **16**, 15339.
- 19 P. Chang, H. Cheng, W. Li, L. Zhuo, L. He, Y. Yu and F. Zhao, *Phys. Chem. Chem. Phys.*, 2014, **16**, 16606.
- 20 N. Zhang, Y. Zhang, X. Pan, X. Fu, S. Liu and Y. J. Xu, *J. Phys. Chem. C*, 2011, **115**, 23501.
- 21 Y. Liu, Y. X. Yu and W. D. Zhang, *J. Phys. Chem. C*, 2013, **117**, 12949.
- 22 Z. Ren, J. Zhang, F. X. Xiao and G. Xiao, *J. Mater. Chem. A*, 2014, **2**, 5330.
- 23 F. X. Xiao, J. Miao and B. Liu, *J. Am. Chem. Soc.*, 2014, **136**, 1559.
- 24 D. D. Chronopoulos, N. Karousis, S. Zhao, Q. Wang, H. Shinohara and N. Tagmatarchis, *Dalton Trans.*, 2014, **43**, 7429.
- 25 F. X. Xiao, J. Miao, H. Y. Wang and B. Liu, *J. Mater. Chem. A*, 2013, **1**, 12229.
- 26 K. Vignesh, R. Priyanka, R. Hariharan, M. Rajarajan and A. Suganthi, *J. Ind. and Eng. Chem.*, 2014, **20**, 435.
- 27 M. Liu, F. Li, Z. Sun, L. Ma, L. Xu and Y. Wang, *Chem. Commun. (Camb)*, 2014, **50**, 11004.
- 28 S. Kaveri, L. Thirugnanam, M. Dutta, J. Ramasamy and N. Fukata, *Ceram. Int.*, 2013, **39**, 9207.
- 29 Y. Hu, X. Gao, L. Yu, Y. Wang, J. Ning, S. Xu and X. W. Lou, *Angew. Chem. Int. Ed.*, 2013, **52**, 5636.
- 30 X. Dai, M. Xie, S. Meng, X. Fu and S. Chen, *Appl. Catal. B: Environ.*, 2014, **158-159**, 382.
- 31 Z. Chen, S. Liu, M. Q. Yang and Y. J. Xu, *ACS Appl. Mater. Interfaces*, 2013, **5**, 4309.
- 32 X. Li, G. Zhang, X. Bai, X. Sun, X. Wang, E. Wang and H. Dai, *Nat. Nanotechnol.*, 2008, **3**, 538.
- 33 G. Shi, C. Li, G. Lu, H. Bai and Y. Xu, *J. Am. Chem. Soc.*, 2008, **130**, 5856.
- 34 K. Mullen, L. Zhi and X. Wang, *Nano Lett.*, 2008, **8**, 323.
- 35 C. Lamprecht, I. Liashkovich, V. Neves, J. Danzberger, E. Heister, M. Rangl, H. M. Coley, J. McFadden, E. Flahaut, H. J. Gruber, P. Hinterdorfer, F. Kienberger and A. Ebner, *Nanotechnology*, 2009, **20**, 434001.
- 36 Z. X. Cai, H. Yang, Y. Zhang and X. P. Yan, *Anal. Chim. Acta*, 2006, **559**, 234.
- 37 H. X. Wang, Q. Wang, K. G. Zhou and H. L. Zhang, *Small*, 2013, **9**, 1266.
- 38 Y. Dong, J. Shao, C. Chen, H. Li, R. Wang, Y. Chi, X. Lin and G. Chen, *Carbon*, 2012, **50**, 4738.
- 39 R. E. Offeman and W. S. J. Hummers, *J. Am. Chem. Soc.*, 1958, **80**, 1339.
- 40 N. N. Chai, J. Zeng, K. G. Zhou, Y. L. Xie, H. X. Wang, H. L. Zhang, C. Xu, J. X. Zhu and Q. Y. Yan, *Chem.-Eur. J.*, 2013, **19**, 5948.
- 41 J. He, J. Wang, Y. Chen, J. Zhang, D. Duan, Y. Wang and Z. Yan, *Chem. Commun. (Camb)*, 2014, **50**, 7063.
- 42 S. Saha, G. Das, J. Thote and R. Banerjee, *J. Am. Chem. Soc.*, 2014, **136**, 14845.
- 43 M. H. Jung and M. J. Chu, *Nanoscale*, 2014, **6**, 9241.
- 44 I. V. Lightcap and P. V. Kamat, *J. Am. Chem. Soc.*, 2012, **134**, 7109.
- 45 J. Xiong, Y. Liu, C. Cao, L. Shen, W. i. Wu, Shijing Liang, R. Liang and L. Wu\*, *J. Mater. Chem. A*, 2015, **3**, 6935.
- 46 H. Zhang, H. Huang, H. Ming, H. Li, L. Zhang, Y. Liu and Z. Kang, *J. Mater. Chem.*, 2012, **22**, 10501.
- 47 G. Xie, K. Zhang, H. Fang, B. Guo, R. Wang, H. Yan, L. Fang and J. R. Gong, *Chem.-Asian. J.*, 2013, **8**, 2395.
- 48 P. Eskandari, F. Kazemi and Y. Azizian-Kalandaragh, *Sep. Purif. Technol.*, 2013, **120**, 180.